AIAA 81-1980R

Development of a Sound Radiation Model for a Finite-Length Duct of Arbitrary Shape

M. A. Hamdi* and J. M. Ville†
Université de Technologie de Compiègne, Cedex, France

A new variational formulation by integral equations has been developed to solve Helmholtz's equation with mixed boundary conditions. Contrary to previous methods generally based on the Wiener-Hopf technique which are limited to the case of a circular semi-infinite duct, our method allows the computation of sound radiation from the duct with arbitrary shape and finite length. Experimental works have been conducted using a spinning mode synthesizer. Comparison between theoretical and experimental results of pressure reflection coefficients for two inlet shapes and directivity patterns shows a very good agreement. Differences between results for finite and semi-infinite length ducts are twofold: locations of principal lobe of radiation are not the same, and secondary lobes of radiation arise at a frequency under the cutoff frequency of the first radial mode.

Nomenclature

a = duct radius
$\mathcal{A}$ = bilinear form
D = boom radius
f = velocity potential on source section $S1$
f_0 = frequency
g = duct wall velocity
G = Green's function
k = wave number
L = duct length
m = azimuthal wave number
n = radial number
$|P|$ = normalized linear amplitude of sound pressure, $\rho\omega^2|\varphi|$
$|R|$ = pressure reflection coefficient modulus
$S1$ = source section
$S2$ = duct wall surface
t = time
Δ = Laplace's operator
Θ = polar angle
λ = wavelength
μ = density of double-layer potential on the duct walls
ρ = fluid density
σ = density of single-layer potential on the source section
φ = velocity potential
Ψ = cylindrical angle coordinate
ω = angular frequency
Ω = fluid domain

Introduction

In order to reduce noise radiated from aircraft engine inlets, recent experimental investigations have studied the effect of inlet geometry on sound radiation. A pressure-radiated field has been shown to be very dependent on inlet contour.[1] This work suggested the necessity to develop theoretical studies in order to predict sound radiation from the duct with arbitrary inlet shape, and then to optimize duct geometry to reduce or deviate radiated noise.

Theoretical works are generally based on the Wiener-Hopf technique,[2] which is limited to the case of a semi-infinite length duct with circular cross section. Recently, ray theory[3] has been used to take into account the inlet geometry.

Presented as Paper 81-1980 at the AIAA 7th Aeroacoustics Conference, Palo Alto, Calif., Oct. 5-7, 1981; submitted Oct. 16, 1981; revision received March 22, 1982.

*Research Engineer.
†Assistant Professor.

The purpose of this paper is to present a new variational formulation, which has been developed to predict exact sound radiation from the duct with arbitrary shape and finite length. Experiments have been conducted simultaneously to validate the theory.

Theoretical and experimental results of pressure reflection coefficients and directivity patterns are presented for various modes and frequencies.

Mathematical Formulation

Let us consider a pipe with finite length, arbitrary shape, and infinitely thin walls (Fig. 1). The velocity potential φ, which is considered a harmonic function of time ($\Phi = \varphi e^{-j\omega t}$), is a solution of the following system P of equations.

$$\Delta\varphi + k^2\varphi = 0 \text{ in } \Omega \tag{1}$$

$$(\partial\varphi/\partial n)_{S2} = g \tag{2}$$

$$\varphi_{S1} = f \tag{3}$$

$$\lim R(\partial\varphi/\partial R - jk\varphi) = 0 \tag{4}$$

Equation (1) is the Helmholtz equation; Eqs. (2) and (3) are boundary conditions on the duct walls, $S2$, and the source section, $S1$, respectively; and Eq. (4) is Sommerfeld's radiation condition.

To solve system P, the velocity potential is expressed as

$$\varphi(M) = \int_{S1} \sigma(P)G(M,P)\,dS1(P) - \int_{S2} \mu(P)\frac{\partial G(M,P)}{\partial np}\,dS2(P) \tag{5}$$

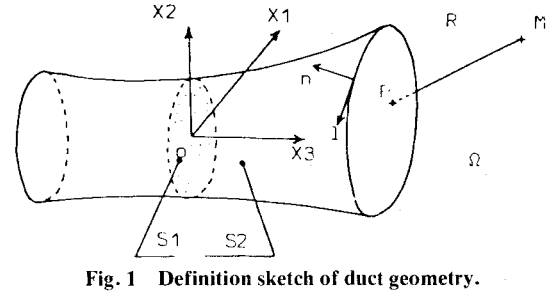

Fig. 1 Definition sketch of duct geometry.

where σ and μ are densities of a single-layer potential on the source section and a double-layer potential on the duct walls, respectively. $G(M,P)=e^{jkR}/4\Pi R$ is the elementary Green's solution which satisfies Eqs. (1) and (4).

It is easy to verify that φ given by Eq. (5) simultaneously satisfies Helmholtz's Eq. (1) and Sommerfeld's condition (4), and that μ and σ represent the jumps of φ through $S2$ and its normal derivative through $S1$, respectively.

$$\mu=[\varphi] \text{ on } S2 \tag{6}$$

$$\sigma=\left[\frac{\partial\varphi}{\partial n}\right] \text{ on } S1 \tag{7}$$

Boundary conditions (2) and (3) yield to a system of two integral equations with unknowns σ and μ:

$$\begin{aligned} f(M) &= \int_{S1}\sigma(P)G(M,P)\,dS1(P) \\ &\quad -\int_{S2}\mu(P)\frac{\partial G(M,P)}{\partial n_p}dS2(P) \qquad M\in S1 \\ g(M) &= \int_{S1}\sigma(P)\frac{\partial G(M,P)}{\partial n_M}dS1(P) \\ &\quad -\mathrm{FP}\int_{S2}\mu(P)\frac{\partial^2 G(M,P)}{\partial n_M\partial n_p}dS2(P) \qquad M\in S2 \end{aligned} \tag{8}$$

Instead of directly solving system (8) with the collocation method, we use a variational formulation that avoids the explicit evaluation of the finite part (FP).

Indeed, system (8) is equivalent to the following variational equation:

$$\begin{aligned} \mathfrak{A}[(\sigma,\mu),(\sigma',\mu')] &= \int_{S1}f(M)\sigma'(M)\,dS1(M) \\ &\quad -\int_{S2}g(M)\mu'(M)\,dS2(M) \\ &\quad \forall\sigma'(M) \text{ on } S1 \text{ and } \mu'(M) \text{ on } S2 \end{aligned} \tag{9}$$

where $\mathfrak{A}$ is the bilinear form given by

$$\begin{aligned} &\mathfrak{A}[(\sigma/\mu),(\sigma'/\mu')] \\ &= \int_{S1}\int_{S1}\sigma(P)G(M,P)\sigma'(M)\,dS1(P)\,dS1(M) \\ &\quad +\int_{S2}\int_{S2}\mu(P)\frac{\partial^2 G(M,P)}{\partial n_M\partial n_p}\mu'(M)\,dS2(P)\,dS2(M) \\ &\quad -\int_{S1}\int_{S2}\mu(P)\frac{\partial G(M,P)}{\partial n_p}\sigma'(M)\,dS2(P)\,dS1(M) \\ &\quad -\int_{S2}\int_{S1}\sigma(P)\frac{\partial G(M,P)}{\partial n_M}\mu'(M)\,dS1(P)\,dS2(M) \end{aligned} \tag{10}$$

Using the property of symmetry of Green's function $G(M,P)$, it can be shown that the bilinear form $\mathfrak{A}$ is symmetric and, therefore, system (8) is given by the stationarity of the functional

$$\begin{aligned} \mathfrak{L}[(\sigma,\mu),(\sigma,\mu)] &= \tfrac{1}{2}\mathfrak{A}[(\sigma,\mu),(\sigma,\mu)] \\ &\quad -\int_{S1}f(M)\sigma(M)\,dS1(M)-\int_{S2}g(M)\mu(M)\,dS2(M) \\ &\quad \sigma(M) \text{ on } S1 \text{ and } \mu(M) \text{ on } S2 \end{aligned} \tag{11}$$

As shown in Refs. 4 and 5, using properties of $\partial^2 G(M,P)/\partial n_M\partial n_p$ the singular integral

$$I=\int_{S2}\int_{S2}\mu(M)\frac{\partial^2 G(M,P)}{\partial n_M\partial n_p}\mu(P)\,dS2(P)\,dS2(M) \tag{12}$$

appearing on the right-hand side of Eq. (10) is also given by

$$\begin{aligned} I &= \int_{S2}\int_{S2}k^2\langle n_M,n_p\rangle G(M,P)\mu(P)\mu(M)\,dS2(P)\,dS2(M) \\ &\quad -\int_{S2}\int_{S2}\langle n_p,\nabla_p\wedge U(M,P)\rangle\mu(P)\mu(M)\,dS2(P)\,dS2(M) \end{aligned} \tag{13}$$

where $U(M,P)$ is the vectorial function

$$U(M,P)=n_M\wedge\nabla_M G(M,P) \tag{14}$$

With Stokes' formula, the second term of $I=I1+I2$ is transformed into

$$\begin{aligned} I2 &= \int_{S2}\mu(M)\left[\int_{\partial S2}\mu(P)\langle U(M,P),dl\rangle\right]dS2(M) \\ &\quad -\int_{S2}\int_{S2}\langle n_p,\nabla_p\mu(P)\wedge U(M,P)\rangle\mu(M)\,dS2(P)\,dS2(M) \end{aligned} \tag{15}$$

Velocity potential φ has no jump ($\mu=0$) along sideline $\partial S2$ of $S2$; therefore, the first integral on the right-hand side of Eq. (15) vanishes. Thus we have

$$\begin{aligned} I2 &= -\int_{S2}n_p\wedge\nabla_p\mu(P) \\ &\quad \times\int_{S2}\mu(M)\langle n_p\wedge\nabla_M G(M,P)\rangle dS2(M)\,dS2(P) \end{aligned} \tag{16}$$

Using the second form of Stokes' formula, the term in brackets can be transformed into

$$\begin{aligned} &\int_{\partial S2}\mu(M)G(M,P)\,dl \\ &\quad -\int_{S2}\langle n_M\wedge\nabla_M\mu(M)\rangle G(M,P)\,dS2(M) \end{aligned} \tag{17}$$

For the same reason, the integral on sideline $\partial S2$ vanishes; thus we have

$$\begin{aligned} I2 &= \int_{S2}\int_{S2}\langle n_M\wedge\nabla_M\mu(M),n_p\wedge\nabla_p\mu(P)\rangle \\ &\quad \times G(M,P)\,dS2(P)\,dS2(M) \end{aligned} \tag{18}$$

The bilinear form $\mathfrak{A}$ is then given by

$$\mathfrak{A}[(\sigma,\mu),(\sigma,\mu)]$$

$$= \int_{S1}\int_{S1} \sigma(P)G(M,P)\sigma(M)\,dS1(P)\,dS1(M)$$

$$-2\int_{S1}\int_{S2} \mu(P)\frac{\partial G(M,P)}{\partial n_p}\sigma(M)\,dS2(P)\,dS1(M)$$

$$+\int_{S2}\int_{S2} [k^2\langle n_M,n_p\rangle\mu(p)\mu(n)$$

$$-\langle n_p\wedge\nabla_p\mu(P),n_M\wedge\nabla_M\mu(M)\rangle]G(M,P)\,dS2(P)\,dS2(M) \tag{19}$$

where μ vanishes on the sidelines of S2.

Finally, discretization with boundary finite element method of Eqs. (11) and (5) provides the solution of the system P.

Numerical Computation

A discretization by boundary finite element method of variational equation (11) yields to a complex symmetrical algebraic system with unknowns σ and μ.

$$\begin{bmatrix} B & C \\ C^T & D \end{bmatrix}\begin{Bmatrix} \sigma \\ \mu \end{Bmatrix} = \begin{Bmatrix} F \\ G \end{Bmatrix} \tag{20}$$

where:

B = matrix associated to single-layer potential on $S1$
D = matrix associated to double-layer potential on $S2$
C = interaction matrix between single- and double-layer potentials on $S1$ and $S2$
$\begin{Bmatrix} F \\ G \end{Bmatrix}$ = vector associated to source terms
$\begin{Bmatrix} \sigma \\ \mu \end{Bmatrix}$ = vector associated to nodal unknowns

Finally, the resolution of system (20) and the discretization of Eq. (5) allows the computation of velocity potential $\varphi(M)$ at any point M of the fluid domain Ω.

Experimental Setup and Data Treatment

Sound radiation from an unflanged circular duct (Fig. 2) has been measured as a function of frequency and modal propagation.

The duct section is 0.45 m long and has an 0.15 m diam. The source section is made of a spinning mode synthesizer[7] with nine acoustic drivers equispaced circumferentially at the duct axial center section. Each acoustic driver is located 1.20 m away from the duct centerline and is connected to the wall with a 2.54-cm diam pipe in order not to modify the acoustic field radiated by both sides of the duct.

The duct and its support are set up in a small anechoic room that measures 3 m large by 2.5 m deep by 2.5 m high.

Amplitude and phase of the signal to the acoustic drivers are achieved by power amplifiers and phase shifter generators, respectively.

A ¼-in. diam condenser microphone mounted on a traversing boom provides measurement of pressure fields. This microphone is traversed in a horizontal arc at an 0.5 m radius from a point 0.05 m in front of a face of the duct on its centerline.

A phasemeter and measuring amplifier connected to plotters provide a phase and amplitude variation of directivity patterns as a function of polar angle from 0 to 90 deg.

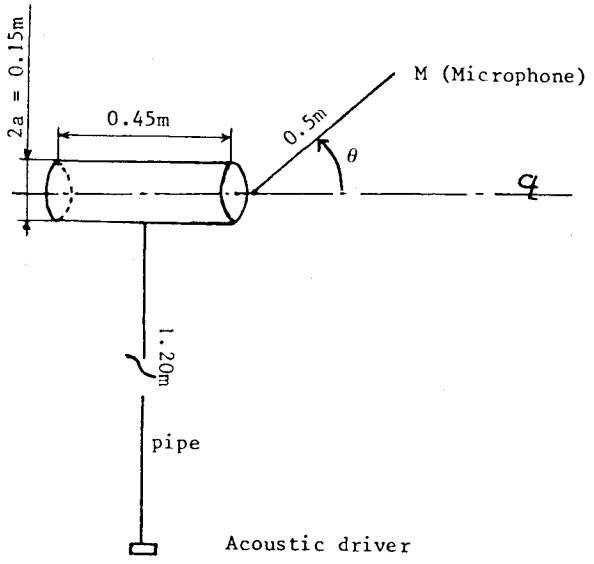

Fig. 2 Sketch of the experimental setup.

Table 1 Experimental test configuration

m	n	ka	f, Hz	Fig. No.
0	0	2	1443	5
0	0	2.4	1732	6
0	0	3.15	2272	7
1	0	2	1443	11
1	0	2.4	1732	12
1	0	3.15	2272	13
2	0	3.15	2272	
2	0	4.5	3247	
2	0	5.2	3751	
3	0	4.5	3247	
3	0	5.2	3751	
3	0	5.9	4256	

Acoustic test conditions are presented for various azimuthal wave numbers and frequencies (Table 1). Measurements have been obtained over an azimuthal wave number range of 0 to 3 and a frequency range up to 4000 Hz. Frequencies are chosen in the order of radial modes to be cut off.

Results

Theoretical results of the pressure reflection coefficient and of the radiated field are compared with experimental data obtained by Ville and Silcox[1] at NASA Langley Research Center. In order to compare with the experiment, numerical computation is obtained with a source term $f=Jm[\mathfrak{X}_{mn}(r/a)]e^{im\Psi}$ representative of the experimental modal configuration which propagates in the duct. If comparison between theory and experiment is possible for the pressure reflection coefficient, it is not the case for directivity patterns, because the duct used at Langley was semi-infinite. As is shown later, the effect of finite length of the duct is very drastic on sound radiation.

Pressure Reflection Coefficient

Figure 3 shows a comparison of our theoretical results and Savkar's results and experimental data[1] for several modes and frequencies.

For the case of plane wave, which propagates in a circular unflanged duct, the formulation gives exactly the same values of the pressure reflection coefficient as computed by Savkar. For higher modes, the agreement between our results and experimental data is better than between Savkar's results and

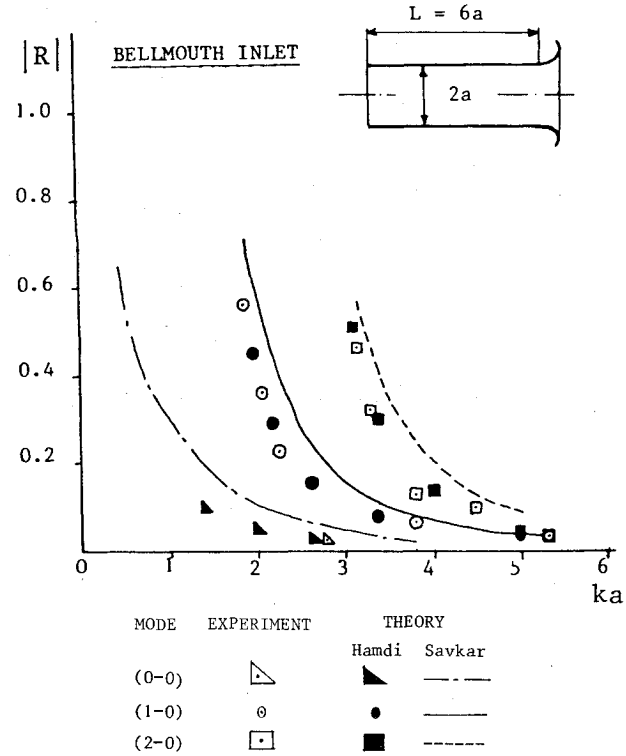

Fig. 3 Pressure reflection coefficient vs frequency parameter (ka) for the unflanged duct case.

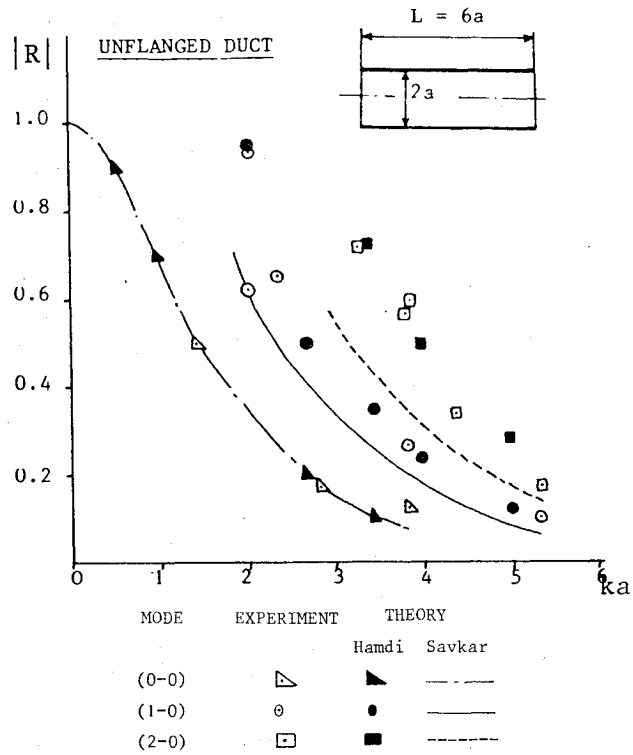

Fig. 4 Pressure reflection coefficient vs frequency parameter (ka) for the bellmouth inlet case.

the same experimental data. We think disagreement between Savkar's results and ours comes from Carrier Koiter's approximation used by Savkar to solve the Wiener-Hopf equation.

Theoretical results of a pressure reflection coefficient are also presented in the case of a circular duct terminated by a bellmouth (Fig. 4). The prediction presented gives agreement with experimental[1] data better than that obtained with Cho's

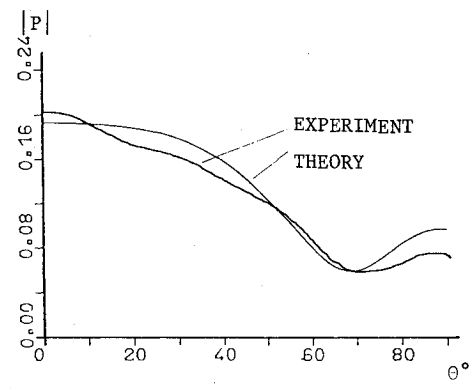

Fig. 5 Amplitude of directivity pattern vs polar angle (mode 0-0, $ka=2$, $D=6.66a$).

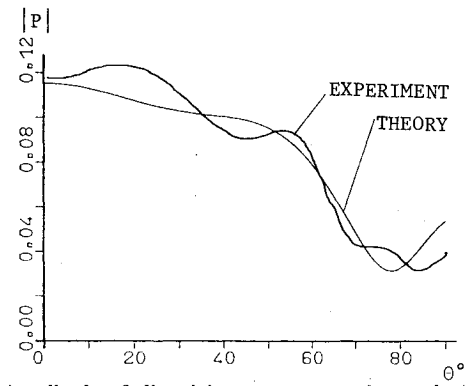

Fig. 6 Amplitude of directivity pattern vs polar angle (mode 0-0, $ka=2.4$, $D=6.66a$).

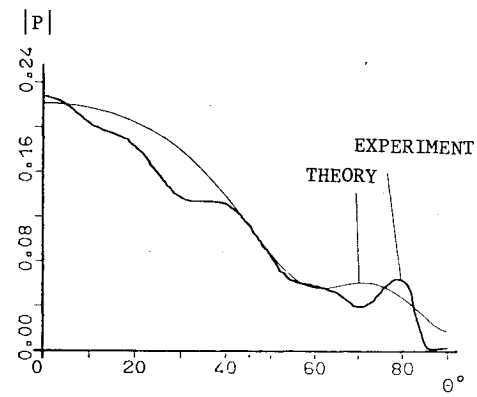

Fig. 7 Amplitude of directivity pattern vs polar angle (mode 0-0, $ka=3.15$, $D=6.66a$).

model,[6] where the 57-deg angle bellmouth inlet is approximated by an infinite hyperboloidal termination.

Radiated Pressure Field

Typical results of the amplitude variation of pressure field radiated from a 0.45 m long unflanged duct vs polar angle are presented.

On Figs. 5-7 experimental and theoretical directivity patterns for the plane wave case and three various frequencies are plotted. The microphone is located $6.66a$ away from the face of the duct. Good agreement is shown between experiment and theory. Minima of pressure are located at polar angles of 66, 78, and 60 deg, for frequency parameters $ka=2$, 2.4, and 3.15, respectively. These phenomena are essentially due to the effect of finite length on sound radiation. Indeed, curves presented in Ref. 1 did not show any results with such pressure extrema because the duct used was semi-infinite.

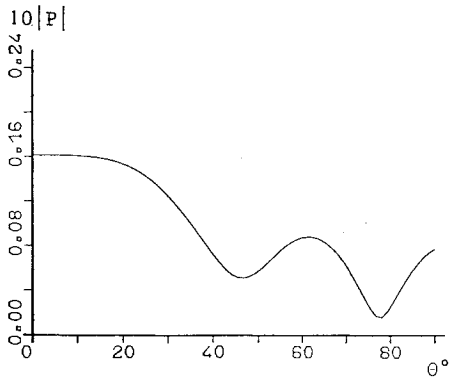

Fig. 8 Theoretical far-field directivity pattern vs polar angle (mode 0-0, $ka = 2$, $D = 100a$).

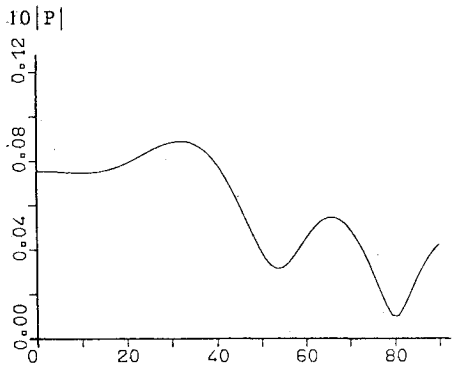

Fig. 9 Theoretical far-field directivity pattern vs polar angle (mode 0-0, $ka = 2.4$, $D = 100a$).

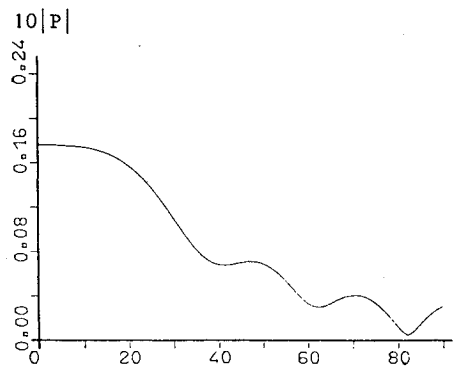

Fig. 10 Theoretical far-field directivity pattern vs polar angle (mode 0-0, $ka = 3.15$, $D = 100a$).

On Figs. 8-10 directivity patterns of the radiated field from the same duct with the same acoustic configurations (plane wave mode) are plotted, but prediction is done at a distance of $100a$. Secondary lobes are still present and even their number is increased. To show that these phenomena are due to the interference between both faces of the duct, it is easy to predict the location of both minima and maxima of pressure with a simple computation. Indeed if we consider the duct is acoustically equivalent to two pistons radiating in phase (source is equispaced from each end of the duct), and located at each end of the duct, angular location of pressure extrema are given by:

$$\Theta_{max} = \arccos\left(p\frac{\lambda}{L}\right) \tag{21}$$

$$\Theta_{min} = \arccos\left(2p+1\right)\frac{\lambda}{2L} \tag{22}$$

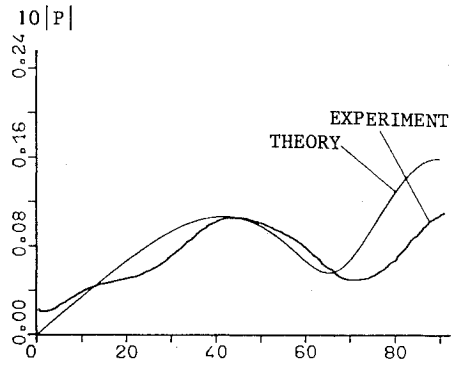

Fig. 11 Amplitude of directivity pattern vs polar angle (mode 1-0, $ka = 2$, $D = 6.66a$).

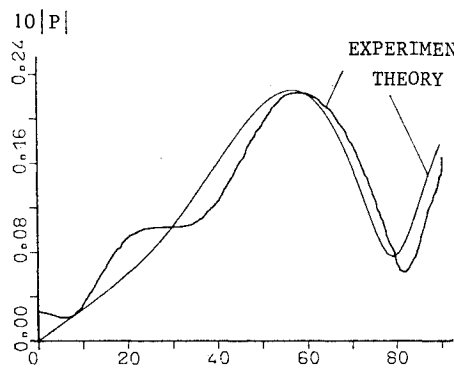

Fig. 12 Amplitude of directivity pattern vs polar angle (mode 1-0, $ka = 2.4$, $D = 6.66a$).

Table 2 Minima and maxima of pressure locations, deg

ka =		2	2.4	3.15
Θ_{min}	Eq. (22)	75	77.4	80.4
		38	49	60
				33.7
	theory	78	80	82
		47	54	63
			0	41
Θ_{max}	Eq. (21)	90	90	90
		58.4	64	70
			29.2	48.3
				4
	theory	90	90	90
		62	66	71
		0	32	47
				0

where p is an integer.

In Table 2 the values of Θ_{max} and Θ_{min} predicted by Eqs. (21) and (22) are presented and compared to theory.

Agreement is good except for the $ka = 2$ case where the far-field approximation is not yet valid.

On Figs. 11-13 directivity patterns (at $D = 6.66a$) are plotted for the first higher-order mode $m = 1$ and frequency parameter $ka = 2$, 2.4, and 3.15, respectively. Again, very good agreement is found between experiment and theory,

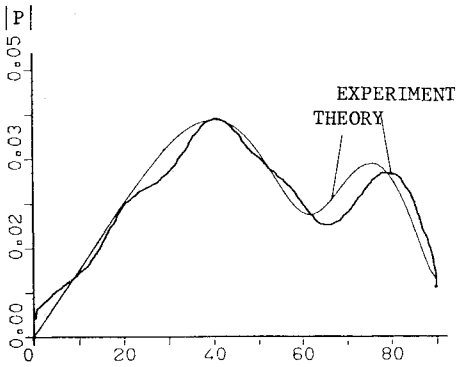

Fig. 13 Amplitude of directivity pattern vs polar angle (mode 1-0, $ka = 3.15$, $D = 6.66a$).

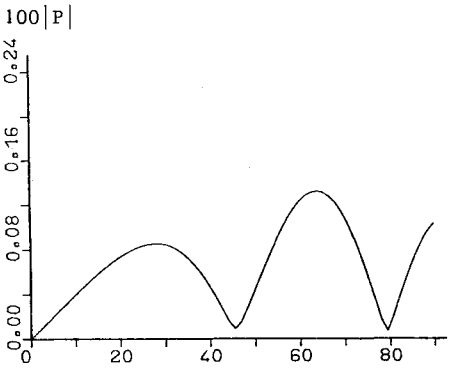

Fig. 14 Theoretical far-field directivity pattern vs polar angle (mode 1-0, $ka = 2$, $D = 100a$).

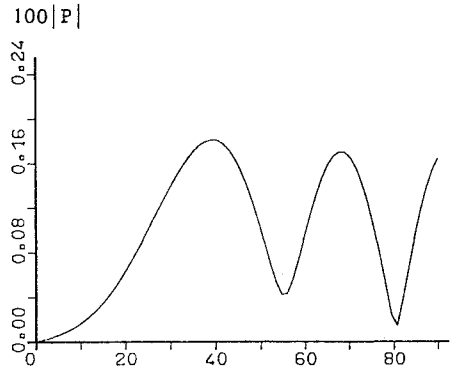

Fig. 15 Theoretical far-field directivity pattern vs polar angle (mode 1-0, $ka = 2.4$, $D = 100a$).

which validates our prediction. As for the plane wave case, secondary lobes are present even in the far field (Figs. 14-16). It has to be pointed out that the minima of pressure are occurring at the same polar angle for the mode case 1 as for the plane wave case. This remark confirms that this phenomenon is due to interference between acoustic waves coming out of two ends of the duct.

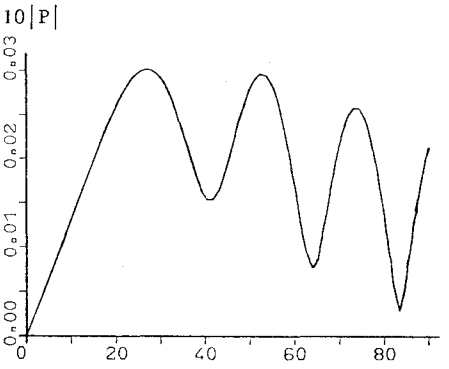

Fig. 16 Theoretical far-field directivity pattern vs polar angle (mode 1-0, $ka = 3.15$, $D = 100a$).

Conclusions

A new variational formulation by integral equations is presented to solve Helmholtz's equation. Discretization of this formulation by boundary finite elements leads to symmetrical matrices. Its application to prediction of sound radiation from finite length inlets of any shape is validated by an experimental investigation.

This theory allows computation of both the complex pressure reflection coefficient and complex directivity patterns.

Effect of finite length on radiated field has been shown to make secondary lobes appear in the far field. This influence can lead to not having a maximum of pressure on the centerline of the duct even for the plane wave case. It has been shown that this phenomenon is essentially due to the interference between the two acoustic waves coming out of both ends of the duct.

In order to reduce or deviate sound radiation from inlets, this formulation will be extended to cases of sound radiation from a duct with lined walls and a duct immersed in a fluid in motion, and will be used to optimize the contour of the intakes.

References

[1] Ville, J. M. and Silcox, R. J., "Experimental Investigation of the Radiation of Sound from an Unflanged Duct and a Bellmouth, Including Flow Effect," NASA TP 1697, Aug. 1980.

[2] Savkar, S. D., "Radiation of Cylindrical Duct Acoustic Modes with Flow Mismatch," *Journal of Sound and Vibration,* Vol. 42, No. 3, Oct. 1975, pp. 363-386.

[3] Kempton, A. J., "Ray Theory to Predict the Propagation of Broadband Fan Noise," AIAA Paper 80-0968, 1980.

[4] Hamdi, M. A., "Une formulation variationnelle par equations intégrales pour la résolution de l'équation de Helmholtz avec des conditions aux limites mixtes," *Compte-rendu à l'Académie des Sciences de Paris,* Vol. 292, Series II, Jan. 1981, pp. 17-20.

[5] Hamdi, M. A., "Formulation variationnelle par Equations Integrales pour le calcul de champs acoustiques proches et lointains," These d'Etat, Université de technologie de Compiegne, Compiegne, France, June 1982.

[6] Cho, Y. C., "Sound Radiation from Hyperboloidal Inlet Ducts," AIAA Paper 79-0677, March 1979.

[7] Perulli, M. and Ville, J. M., "Measurement of Absorbing Materials Acoustic Parameters in the Working Conditions of an Intake Duct," AIAA Paper 77-1332, Oct. 1977.